PAPER

Check for updates

The preparation and physicochemical properties of biodegradable konjac glucomannan-based films reinforced with bacterial cellulose and tea polyphenol for food packaging

Lan Ma,[a] Pengyu Hu,[a] Yihao Zhang,[a] Yunchuan Dai[a] and Yanzhu Guo ⓘ *[ab]

Biodegradable and edible packaging films derived from konjac glucomannan (KGM) are gaining popularity as promising candidates to replace petroleum-based plastics with the aim of alleviating environmental problems. However, their poor mechanical strength and lack of antioxidant activity have restricted their practical application in food packaging. Bacterial cellulose (BC), with a three-dimensional nanostructure and biodegradable and biocompatible properties, was chosen as a reinforcing agent to enhance the mechanical properties of KGM film. Film prepared with 15% BC displayed the highest tensile strength of 62.87 MPa and elongation at break of 38.17%, owing to the strong hydrogen bond interactions between the BC and KGM chains. Furthermore, tea polyphenols (TP), a type of natural antioxidant agent, were incorporated into the BC and KGM composite films and endowed films with excellent antioxidant properties, with scavenging rates toward DPPH and ABTS free radicals of up to 96.74% and 97.50%, respectively. Meanwhile, the mechanical strength, UV shielding performance, and water-vapor and oxygen barrier properties of the films were also improved through the incorporation of TP. The film was successfully applied as a packaging material for fresh-cut apple preservation. The prepared film demonstrated nontoxicity and excellent biodegradability over 28 days, with no significant impact on plant growth. Therefore, the prepared composite film exhibited great prospects as a novel type of biodegradable, sustainable and bioactive film for food preservation.

1 Introduction

As one of the effective barriers against oxygen, moisture, oils and microorganisms, food packaging films can maintain food quality, protect food products from environmental pollution during distribution, retail and storage, and ultimately extend the quality or shelf-life of food.[1] However, large amounts of traditional food packaging films are generally produced with plastic materials, which are generally derived from non-renewable fossil resources and are difficult to degrade, thus exhibiting a negative impact on the ecological environment.[2] Therefore, the development of packaging films using biomass-based polymers as alternatives to plastic has garnered significant research interest. Various natural biopolymers, *e.g.*, proteins,[3] polysaccharides[4] and lipids,[5] have been widely investigated as raw materials for packaging materials due to

their biodegradability, biocompatibility, nontoxicity and accessibility.[6]

As a type of natural water-soluble polysaccharide, konjac glucomannan (KGM) is an ideal raw material for preparing food packaging film, owing to the fact that KGM is generally produced from the perennial herb konjac and displays excellent thickening, film-forming, and gelling abilities, and edibility.[7,8] Up to now, extensive literature reports have focused on preparing films from KGM through aqueous solution-casting,[9] electrostatic spinning,[10,11] microfluidic spinning,[12] and hot-press compression molding[13] methods. Notably, the aqueous solution-casting process is particularly promising due to its simplicity and direct compatibility with industrial-scale techniques, facilitating potential scaling up. To date, the mechanical strength of KGM pure film is in the range of 9.15–29.05 MPa based on previous literature reports;[14,15] this is lower than the required strength from the ISO 527 international standard, which clearly points out that the mechanical strength of food packaging films must be higher than 30 MPa. Therefore, various functional substances, *e.g.*, graphene oxide (GO),[16] mica nanosheets (MN),[17] titanium dioxide nanoparticles (TiO$_2$ NPs),[18] zinc ions (Zn^{2+}),[19] and zeolite Y (ref. 20) have been incorporated into KGM substrates with the aim of improving their mechanical

[a]Liaoning Province Key Laboratory of Paper and Pulp Engineering, Dalian Key Laboratory of High Value Application and Development of Botanical Resources, Key Laboratory of High Value Utilization of Botanical Resources of China Light Industry, Dalian Polytechnic University, Dalian 116034, China. E-mail: guoyz@dlpu.edu.cn
[b]Guangxi Key Laboratory of Clean Pulp & Papermaking and Pollution Control, School of Light Industry and Food Engineering, Guangxi University, Nanning, 530004, China

properties. Although these inorganic materials are beneficial to the enhancement of KGM mechanical strength, numerous concerns have been raised regarding their continuing use in food due to toxicity and biocompatibility issues. Therefore, exploring types of green, non-toxic, edible additives to enhance the mechanical strength of pure KGM films is necessary and important.

Bacterial cellulose (BC) is a type of linear polysaccharide, which is composed of β-D-glucopyranose units ($C_6H_{11}O_5$) with β-1,4-glycosidic bonds as unit linkages.[21] It is a type of exopolysaccharide and can be produced by microorganisms, including *Acetobacter*, *Agrobacterium*, and *Rhizobium*, but it is generally derived from *Acetobacter xylinus*.[22] Different from lignocellulose, BC has high purity and is without non-cellulose components, such as lignin and hemicelluloses, which imparts it with outstanding material plasticity, moisture retention abilities and mechanical performance.[23] Meanwhile, the crystallinity and polymerization degree of BC are up to 70–80% and 2000–10000,[24] respectively, which are generally higher than those of lignocellulose, and this is beneficial for enhancing the mechanical strength of BC-based materials. Furthermore, BC has a unique ultra-fine three-dimension structure, numerous hydroxyl groups, and excellent biodegradability, biocompatibility and edibility. All of these special properties enable BC to potentially function as a matrix or nanofiller in the preparation of food packaging films. In fact, it has been confirmed that the addition of BC as a nanofiller into polysaccharide film matrices—*e.g.* agar,[25] gelatin[26] and chitosan[27]—effectively enhances their mechanical strength, as numerous hydrogen bonds form between the hydroxyl groups in the BC chains and the polysaccharide matrix. These interactions are key to achieving a combination of high strength and moderate flexibility, which is essential for industrial processing, sealing, and wrapping products without cracking. Meanwhile, the introduction of BC into polysaccharide matrices has a positive effect on elevating the barrier performance of films, such as water-vapor permeability (WVP) and oxygen permeability (OP).[28] Moreover, this elevation is helpful for enhancing the actual application of films in food preservation. However, the addition of BC as a nanofiller to KGM matrices to enhance the physicochemical characteristics of films has hardly been studied in the literature. Therefore, one objective of this work is to explore the feasibility and possibility of overcoming the weak mechanical strength of pure KGM films by introducing BC into KGM, and the interactions between them are also investigated.

Antioxidant properties are vital and necessary in food packaging films, as they can effectively inhibit the occurrence or spread of oxidative reactions, thereby preventing the oxidation and browning of nutrients in food.[29] However, it is usually accepted that the above-mentioned KGM and BC are without antioxidant properties. Tea polyphenols (TP), one type of natural antioxidant, are generally extracted from tea and involve a mixture of anthocyanins, flavonoids and phenolic acids.[30] TP are well known for their antioxidant properties and have been evaluated and applied as an antioxidant in food packaging films due to their favourable biocompatibility, non-toxicity, and biodegradability.[31] Their antioxidant properties mainly involve

the chelation of metal ions and scavenging of reactive oxygen species, thereby inhibiting free radical chain reactions.[32] The second objective of this work was to impart KGM and BC composite films with antioxidant properties *via* the incorporation of TP and to investigate the mechanisms of TP release in the composite films.

In this work, environmentally-friendly composite films were fabricated with KGM as the matrix, BC as the nanofiller and TP as the active material *via* a solution casting method, which is a facile and easily-performed approach. The mechanical strength, barrier properties, thermal stability, microstructure, and light transmittance of the prepared KGM-based films were assessed. Additionally, the antioxidant and UV shielding properties of the active films were also evaluated. Finally, KGM-BC-TP films were applied to the preservation of fresh-cut apples, and variations in preservation indicators, including weight loss rate, pH value, colour, browning index (BI), polyphenol oxidase enzyme (PPO) activity and total titratable acidity (TTA), were examined. Ultimately, this study aimed to develop packaging film that not only demonstrates high performance in the laboratory but also was designed with industrial packaging in mind, simultaneously addressing the key challenges of scalability, transparency, flexibility, and biodegradability in integrated, active food preservation.

2 Experiment

2.1. Materials

Konjac glucomannan (KGM, food grade) was purchased from Jilida Food Co., Ltd (Dalian, China). The bacterial cellulose suspension (BC, 3.5 wt%) was purchased from Alpha Biotech Co., Ltd (Dalian, China), and it was produced through the fermentation of *Komagataeibacter* sp. ATC301 in culture solution (containing glucose, sucrose, corn syrup, *etc.*) by a dynamic cultivation method. Glycerol (GL, ≥99.5% purity) and tea polyphenols (compound, 98% purity) were acquired from Aladdin Biochemical Technology Co., Ltd (Shanghai, China), while gallic acid monohydrate (AR, 98.5% purity), 2,2′-azino-bis(3-ethylbenzothiazoline-6-sulfonic acid) diammonium salt (ABTS, 98% purity), 2,2-diphenyl-1-picryl-hydrazyl (DPPH, ≥98.5% purity), and Folin–Ciocalteu's phenol reagent (1 N) were provided by Macklin Biochemical Co., Ltd (Shanghai, China). Anhydrous calcium chloride ($CaCl_2$, ≥96.0% purity) was purchased from Guangdong Guanghua Sci-Tech Co., Ltd (Shantou, China). Barium chloride dihydrate ($BaCl_2 \cdot 2H_2O$, ≥99.5% purity) and potassium carbonate (K_2CO_3, ≥99.0% purity) were provided by Tianjin Damao Chemical Reagent Co., Ltd (Tianjin, China). Seasonal cabbage seeds were provided by Huayu Biotechnology Co., Ltd (Yangxin, China). Deionized water was prepared in the laboratory.

2.2. Preparation of KGM-BC films and KGM-BC-TP films

Approximately, 0.70 g of KGM and 0.21 g of glycerol (functioning as a plasticizer) were dispersed into 70 mL of deionized water in a flask, which was then stirred magnetically at 400 rpm and 95 °C for 60 minutes to generate the transparent KGM

aqueous solution. The added amount of BC was calculated based on the weight of KGM. In detail, when the actual amount of BC suspension was 0, 1, 2, 3, 4, and 5 g, the corresponding BC content levels (w/w) in solution were marked as 0%, 5%, 10%, 15%, 20%, and 25%, respectively. The predetermined weight of bacterial cellulose (BC) suspension was then added into the above-prepared solution and the mixtures were then stirred by a high-speed shearing machine (T18, IKA, Germany) at 10 000 rpm for 3 minutes. The BC content varied from 0% to 25%, and the prepared KB composite films were denoted as KGM, KB_5, KB_{10}, KB_{15}, KB_{20}, and KB_{25} (w/w, based on the dry weight of KGM in the mixture), respectively. Subsequently, the solutions were then centrifuged at 2800 rpm for 4 minutes to remove air bubbles in the solutions, which were evenly distributed into 12 × 12 cm Petri dishes and subsequently dried in an oven at 40 °C for 12 hours. The resulting films were stored at 25 °C for 48 hours in a desiccator containing saturated potassium carbonate before further testing.

2.3. Preparation of KGM-BC-TP films

Firstly, KGM solution with 15% BC content was prepared by the above procedures. Certain amounts of TP were dissolved in 3 mL of deionized water under mechanical stirring for 3 minutes at room temperature. The amount of TP was calculated based on the weight of KGM. In detail, when the actual amount of TP was 0.007, 0.021, 0.035, 0.049, and 0.063 g, the corresponding TP content levels (w/w) in solution were marked as 1%, 3%, 5%, 7%, and 9% respectively. The resulting TP solutions were then added to the KGM and BC mixed solutions and vigorously stirred at 10 000 rpm for 3 minutes by a high-speed shearing machine (T18, IKA, Germany). After degassing, the mixed solutions were then poured into Petri dishes (12 × 12 cm). The KGM-BC-TP films (KBT) were obtained after drying the solutions in an oven at 40 °C for 12 hours and their storage conditions were similar to those of KB films. KBT films with 1%, 3%, 5%, 7% and 9% TP content (the percentage dry weight of TP to KGM) were prepared, which were called KBT_1, KBT_3, KBT_5, KBT_7, and KBT_9, respectively. For comparison purposes, KB film without the addition of TP was also prepared and called KB_{15}.

2.4. Characterization

The surface and cross-sectional morphologies of the KGM, KB and KBT films were observed using a scanning electron microscope (JSM-7800F, Japan Electronics Co., Ltd, Japan), while their FT-IR spectra were recorded with a spectrometer (Frontier I, PerkinElmer Instruments, USA). The XRD patterns of the prepared films were analysed using an X-ray diffractometer (XRD-6100, Shimadzu, Japan) at room temperature, and they were scanned from 10° to 50° at 0.02° intervals using Cu Kα radiation as the source. The thermal stability of the films was characterized using a thermo-gravimetric analyser (TGA Q500, TA Instruments, USA) under a nitrogen atmosphere at a flow rate of 40 mL min^{-1}. The mechanical properties of the films (2 cm × 10 cm) were evaluated using an electronic universal testing machine (XLW-PC, Jinan Languang Electromechanical Technology Co., Ltd, China). Film thickness was measured

using a micrometer (IP65, Weidu, China); measurements were performed at six different points on the films and the average thickness was calculated. Surface wettability was evaluated by measuring the water contact angle (WCA) with an analyser (Model ABL100040, Biolin Scientific, Finland). In brief, a water droplet (3 μL) was deposited onto the film surface, and the static angle was recorded after 5 s at 25 °C. The WCA values of film samples were obtained by measuring at five random positions on the films and then calculating the average. The rheological behaviour of the film-forming solution was assessed using a dynamic rheometer (HR10, TA Instruments, USA) within a shear rate range of 0.1 to 100 s^{-1}.

2.5. Barrier properties

The water vapor permeability (WVP) and oxygen permeability (OP) of films were characterized referring to the existing literature.[33] Generally, 26 g of anhydrous calcium chloride was first dried in a 105 °C oven for 2 h and then placed into a 50 mL centrifuge tube. The film was trimmed into discs with a diameter of 40 mm and sealed with double-sided tape in the mouth of the centrifuge tube. The centrifuge tube was then transferred into a desiccator containing saturated barium chloride solution and it stood for 48 hours at room temperature. The thickness of the film and the weight of the tube before and after treatment were determined and the WVP of films was calculated using the following equation:

$$\text{WVP} = \frac{m \times d}{A \times t \times p} \tag{1}$$

where m represents the change in the weight of the centrifuge tube after treatment (g); t represents the interval between two measurements (s); d refers to the film thickness (mm); A represents the area which water vapor passed through (m^2), and p represents the difference in water vapor pressure across the film (Pa).

The oxygen permeability (OP) of the films was determined using the deoxidizer adsorption method.[33] In general, 1.5 g of sodium chloride, 1.0 g of activated carbon and 0.5 g of reduced iron powder, which were employed as the deoxidizing agents, were added into a 50 mL centrifuge tube. The centrifuge tubes were sealed with the film sample and stored in a desiccator containing saturated potassium chloride solution at ambient temperature for 48 hours. The initial and final weights of the tube were derived and the OP was calculated by formula (2):

$$\text{OP} = \frac{m_1 - m_0}{t \times A} \tag{2}$$

where m_0 and m_1 denote the initial and final weights of the centrifuge tube (g); t refers to the interval time (s), and A indicates the effective area of the film (cm^2).

2.6. Water sensitivity

The water sensitivity of the films was analysed by determining their moisture content (MC) and water solubility (WS). Film samples with dimensions of 4 cm × 4 cm were initially prepared and accurately weighed (m_1); they were then dried at 105 °C until they reached a constant weight (m_2). Subsequently,

the dried film samples were immersed in 50 mL of deionized water at room temperature where they stood for 24 hours. After immersion, the film samples were re-dried at 105 °C for 24 hours, and their final weight (m_3) was recorded. The measurements were conducted in triplicate. MC and WS were analysed according to eqn (3) and (4), respectively:

$$MC = \frac{m_1 - m_2}{m_1} \times 100 \quad (3)$$

$$WS = \frac{m_2 - m_3}{m_2} \times 100 \quad (4)$$

2.7. UV-vis spectroscopy and film colour

The optical characteristics of the films were evaluated using a spectrophotometer (UH-5300, Hitachi, Japan), and their UV-vis spectra were collected within the range of 200–800 nm. Additionally, the opacity of the films at 600 nm was determined using eqn (5):[34]

$$Opacity = -\frac{\log T_{600nm}}{d} \quad (5)$$

where T_{600nm} represents the transmittance of the film at a wavelength of 600 nm, and d denotes the thickness of the film (mm).

The percentages of UVA (320–400 nm) and UVB (280–320 nm) blocking were calculated from the transmittance data and eqn (6) and (7):

$$UVA\ blocking(\%) = \frac{\int_{320}^{400} T(\lambda)d\lambda}{\int_{320}^{400} d\lambda} \quad (6)$$

$$UVB\ blocking(\%) = \frac{\int_{280}^{320} T(\lambda)d\lambda}{\int_{280}^{320} d\lambda} \quad (7)$$

where $T(\lambda)$ represents the average transmittance of the film at a wavelength of λ, d(λ) represents the bandwidth, and λ is the wavelength.

The colorimetric properties of the film samples were measured using an automatic colorimeter (NR10 QC, Shenzhen 3nh Technology Co., Ltd, China), which quantified three key chromaticity parameters: L^* (representing the lightness gradient), a^* (denoting a chromatic shift toward red (+value) or green (−value)), and b^* (indicating the yellow (+value) or blue (−value) intensity). The total colour difference (ΔE^*), a crucial indicator of visual perceptibility, was then determined using standardized colorimetric calculations to provide a comprehensive assessment of material-related chromatic changes. The total colour variation (ΔE^*) was calculated using eqn (8):

$$\Delta E^* = \sqrt{(\Delta L^*)^2 + (\Delta a^*)^2 + (\Delta b^*)^2} \quad (8)$$

where ΔL^*, Δa^* and Δb^* represent the variations in brightness, red-green shift and yellow-blue intensity, respectively; these deviations are calculated relative to a standardized white reference ($L = 98.39$, $a = -0.14$, and $b = 0.8$).

2.8. Determination of the total phenolic content and antioxidant activity

The antioxidant activities of the films were assessed using DPPH and ABTS free-radical scavenging assays.[35] Film samples (4 cm × 4 cm) were immersed in 10 mL of deionized water for 24 hours. The resulting mixtures were then centrifuged at 3000 rpm for 5 minutes, and the supernatants were collected for the determination of the total phenolic content (TPC) and subsequent free radical scavenging analysis. Different supernatants (200 μL) were then mixed with 5 mL of Folin–Ciocalteu phenol reagent and they reacted for 5 minutes. Additionally, 4 mL of 7.5% (w/v) sodium carbonate solution was added to the above mixtures, and the absorbance values at 765 nm of the solutions after reacting for 1 hour were determined using a spectrophotometer. According to a previously reported method,[36] a standard curve between the gallic acid concentration and its absorbance at 765 nm was established. Subsequently, the TPC in different solutions could be obtained by relating their absorbance to the standard curve of gallic acid.

In the DPPH analysis process, 200 μL of supernatant was added to 3 mL of DPPH solution (50.0 μg mL^{-1} in ethanol solution), and this was kept in the dark at 25 °C for 30 minutes. The absorbance of the sample solution at 517 nm was recorded using a spectrophotometer (UV-1200, Shanghai Meishi Instrument Co., Ltd, China). A blank sample including 200 μL of deionized water and 3 mL of DPPH ethanol solution (50.0 μg mL^{-1}) and a control sample composed of 200 μL of deionized water and 3 mL of anhydrous ethanol were also prepared. The absorbance values of these two solutions at 517 nm were also collected and the DPPH radical scavenging activities of films were calculated using eqn (9):

$$DPPH\ scavenging\ ratio(\%) = \left(1 - \frac{A_s - A_c}{A_b}\right) \times 100 \quad (9)$$

where A_s, A_c and A_b represent the absorbance of the sample, control and blank solutions, respectively.

In the ABTS analysis process, 200 mg of ABTS and 34.4 mg of potassium persulphate were first dissolved into 50 mL of 95% (v/v) ethanol solution to produce ABTS solution. The above-prepared solution was then diluted with 95% (v/v) ethanol buffer until its absorbance at 734 nm was constant at 0.70 ± 0.02. Subsequently, 200 μL of supernatant was mixed with 3 mL of diluted ABTS solution, which was further treated for another 5 minutes in the dark. Thereafter, the absorbance at 734 nm was then measured. A blank group was also prepared by combining 3 mL of the diluted ABTS solution with 200 μL of deionized water. The ABTS radical scavenging activities of the samples were calculated by eqn (10):

$$ABTS\ scavenging\ ratio(\%) = \left(\frac{A_b - A_s}{A_b}\right) \times 100 \quad (10)$$

where A_b and A_s represent the absorbance of the blank and sample solutions, respectively.

2.9. Release testing

According to the method proposed by Yi *et al.*,[36] release testing was carried out using 50% (v/v) ethanol solution and deionized water as a food simulant. Briefly, films with predetermined weights and dimensions (4 cm × 4 cm) were immersed in 10 mL of ethanol (50%, v/v) solution or deionized water at room temperature. At the designated time, 1 mL of sample solution was taken out for further analysis and 1 mL of ethanol solution (50%, v/v) or water was supplemented into the tube to maintain the total volume of solution at 10 mL. The collected sample solution was then mixed with 5 mL of Folin–Ciocalteu's phenol reagent and allowed to react for 5 minutes. Additionally, 4 mL of 7.5% (w/v) sodium carbonate solution was added into the above mixture, and the absorbance at 765 nm of the solution after reacting for 1 hour was determined using a spectrophotometer. The concentration of TP in solution was expressed as gallic acid equivalents based on the gallic acid standard curve following a previously reported method.[36] The cumulative release efficiency of TP was calculated by eqn (11):

$$\text{Cumulative release efficiency(\%)} = \frac{C_n \times V + \sum_{i=0}^{n-1} C_i \times V_i}{m} \times 100 \tag{11}$$

where C_n represents the concentration of TP at the designated time ($\mu g\ mL^{-1}$); V represents the total volume of the sample solution (mL); V_i represents the volume of sample solution removed at the designated time (mL); C_i represents the concentration of TP at the designated time ($\mu g\ mL^{-1}$), and m represents the total weight of TP in the film (μg).

The TP release data was fitted using Ritger–Peppas[37] and Peppas–Sahlin[38] models to characterize the release mechanism based on the following eqn (12) and (13):

$$\frac{M_t}{M_\infty} = kt^n \tag{12}$$

$$\frac{M_t}{M_\infty} = k_1 t^m + k_2 t^{2m} \tag{13}$$

where M_t (mg) represents the amount of TP released into the food simulant at a given time, M_∞ (mg) denotes the total TP amount in the film, t (h) is the time required for the release process, k indicates the release efficiency constant, and n is the release exponent. Similarly, k_1, k_2 and m are the constants for Fickian diffusion, matrix erosion, and the Fickian diffusion exponent, respectively.

2.10. Preservation testing using fresh-cut apples

2.10.1. Fruit treatment.
Fresh "Fuji" apples with comparable ripeness and quality were purchased from a local market. The apple surfaces were disinfected using sodium hypochlorite solution (200 $\mu g\ L^{-1}$) for 2 minutes, and then rinsed with deionized water. Afterwards, the apples were peeled and cored using a sterilized knife and sliced into 4 cm × 4 cm slices with a thickness of 5 mm. Every fresh-cut apple slice was enclosed in

KB_{15}, KBT_5, and PE film. Unenclosed fresh-cut apples served as the control group. All samples were stored at 4 °C and analysed daily.

2.10.2. Measurement of weight loss and browning index (BI).
All samples were removed from the refrigerator at each sampling time point, weighed and analysed using the following eqn (14):

$$\text{Weight loss(\%)} = \frac{m_1 - m}{m_1} \times 100 \tag{14}$$

where m_1 and m represent the initial weight and weight after the storage period (g), respectively, of the fresh-cut apples.

The surface color of fresh apple slices was evaluated using a colorimeter to obtain the L^*, a^* and b^* values. The BI was then determined according to calculations done using eqn (15) and (16):[39]

$$\text{BI} = \frac{X - 0.31}{0.172} \times 100 \tag{15}$$

$$X = \frac{a^* + 1.75L^*}{5.645L^* + a^* - 3.012b^*} \tag{16}$$

where X is the chromaticity coordinates.

2.10.3. Analysis of pH, total titratable acidity (TTA) and polyphenol oxidase (PPO) enzymes.
Briefly, 10 g of apple sample was ground in a mortar, squeezed and filtered to obtain apple juice. The pH variability was determined using a pH meter (PHS-2F, Rex laboratory pH meter, China) and the average value was obtained after three repetitions.

The total titratable acidity (TTA) values of apple samples were determined on the basis of acid–base neutralization.[40] Approximately, 10 g of milled apple sample was first dispersed in 100 mL of distilled water and filtered through a 0.22 μm filter. Subsequently, 2 or 3 drops of phenolphthalein indicator were added into the filtrate, which was titrated with 0.1 M NaOH solution. The TTA (%) was expressed as a percentage of malic acid and calculated by the following equation:

$$\text{TTA(\%)} = \frac{V \times c \times (V_1 - V_0) \times 0.067}{V_S \times m} \tag{17}$$

where V (mL) represents the total volume of the extracted apple sample, V_S (mL) corresponds to the filtrate volume used for titration, c (mol L^{-1}) indicates the NaOH molar concentration, V_1 (mL) and V_0 (mL) denote the volumes of NaOH used during filtrate titration and blank titration with distilled water, respectively, and m (g) indicates the mass of the analysed sample; 0.067 is the equivalent weight of malic acid.

The detection of polyphenol oxidase (PPO) in fresh-cut apples was done referring to previous studies with minor modification.[40] Briefly, 5 g of sample was weighed and ground, and it was then dispersed into 20 mL of phosphate buffer solution. After stirring in a magnetic stirrer, the mixture was centrifuged at a speed of 6000 rpm for 10 minutes. After centrifugation, 1 mL of the supernatant was mixed with 3 mL of phosphate buffer containing 500 mmol L^{-1} catechol. Its absorbance at 420 nm was measured, and this was repeated three times.

2.11. Biodegradability testing

The biodegradability of KB_{15} and KBT_5 films was evaluated according to a previous method.[41] Specifically, the composite film samples (4×4 cm) were buried in outdoor soil at a depth of 10 cm ($\sim$10–25 °C, 35–65% RH, April 2025, Dalian). The film samples were then taken from the soil and their shapes were photographed every 7 days to determine their biodegradability. In comparison, commercial polyethylene (PE) film was also treated using the same procedure. The mass loss, tested once every week, was calculated using the following eqn (18):

$$\text{Mass loss}(\%) = \frac{m_0 - m_1}{m_0} \times 100 \qquad (18)$$

where m_0 and m_1 are the initial and post-degradation dry masses of the film sample, respectively, measured before burial and after retrieval, upon cleaning with anhydrous ethanol and drying to a constant weight.

2.12. Cytotoxicity testing

Mouse embryonic fibroblasts (3T3) and human umbilical vein endothelial cells (HUVEC) were purchased from Jiangsu Key-GEN BioTECH Co., Ltd (Nanjing, China). The specific catalog numbers are KGG1305-1 for the 3T3 cells and KG419 for the HUVEC cells. The 3T3 cells were cultured in high-glucose Dulbecco's Modified Eagle's Medium (DMEM) supplemented with 10% calf serum (CS), while the HUVEC cells were maintained in high-glucose DMEM containing 10% fetal bovine serum (FBS), also obtained from the same supplier. These two types of cells were cultured at 37 °C under a humidified atmosphere with 5% CO_2. Subsequently, the cells were co-cultured with film samples in 96-well plates for 24 h. After treatment with MTT solution (0.5 mg mL^{-1}) and further incubation, cell viability was assessed according to a previously reported method.[42]

The morphologies of 3T3 and HUVEC cells after co-incubation with film samples were also observed using a confocal laser scanning microscope (LSM880, Carl Zeiss Jena, Germany). Before observation, the cells were stained with calcein acetoxymethyl ester (2 μM) and propidium iodide (4.5 μM) and washed with PBS buffer solution three times.

2.13. Seed germination experiments

The toxicity of films was analysed in the soil that was used to perform the film degradation earlier.[43] Subsequently, a certain weight of soil was placed in a trapezoidal flowerpot, and 30 seeds of seasonal cabbage were evenly buried in the soil. After planting, the soil was regularly watered with 30 mL of water every day. The germination rate and plant height of the seasonal cabbage were measured every week.

2.14. Statistical analysis

All experiments were conducted in triplicate, and the results are presented as means $\pm$ standard deviation (SD). Statistical significance ($p < 0.05$) was determined by one-way ANOVA followed by Duncan's test using SPSS (v27.0, IBM, USA). Graphs and error bars were produced using Origin 2021 software (OriginLab, Northampton, USA).

3 Results and discussion

3.1. Structural characterization and mechanical and barrier properties of KB films

KGM-BC-TP composite films were prepared using a casting method to overcome the low mechanical strength and poor antioxidant and water-resistance properties of pure KGM films. The detailed procedure for the preparation of the KGM-BC-TP (KBT) films is depicted in Fig. 1. As a type of natural polysaccharide with favourable degradability and biocompatibility, KGM was used as the substrate. BC, a type of ultra-fine fibril with a three-dimensional structure and high mechanical stability, was used as a reinforcing agent with the aim of elevating the mechanical strength of the KGM films. TP, as a type of natural active agent, were incorporated into the KGM film to impart it with antioxidant activity. Meanwhile, hydroxyl groups in the TP could interact with the KGM matrix to form hydrogen bonds and thus enhance the mechanical strength of the film.

To confirm the effect of BC on the mechanical properties of the KGM films, KGM and BC composite (KB) films with various BC weight ratios were prepared and their tensile strength (TS) and elongation at break (EAB) were measured. As shown in Fig. 2a and b, the weight ratio of BC to KGM led to significant ($p < 0.05$) differences in the TS and EAB values of the KB films. As the BC content increased from 0% to 15%, the tensile strength of KB film was elevated from 28.20 ± 0.78 MPa to 62.87 ± 1.06 MPa, which was probably due to the formation of large numbers of hydrogen bonds between BC and KGM. The formation of hydrogen bonds could be confirmed based on the FT-IR results in Fig. 2c. In the FT-IR spectrum of KGM, the peak at 3434 cm^{-1} is attributed to stretching vibrations of hydroxyl groups. In the FT-IR spectra of the KB films, this peak displayed a shift towards lower wavenumbers upon increasing the weight ratio of BC to KGM from 0 to 25%. This phenomenon was possibly attributed to the interaction of hydroxyl groups between BC and KGM. These interactions could generate hydrogen bonds between the BC and KGM molecules and thus
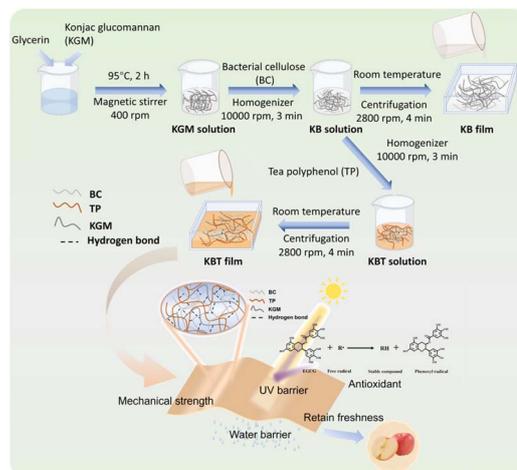

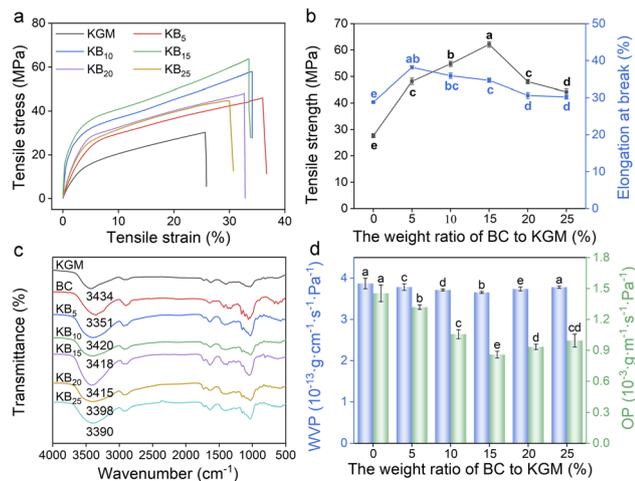Fig. 1 A schematic diagram of the preparation of KBT films.

Fig. 2 Tensile stress−strain curves of KB films (a); the effect of BC dosage on the mechanical properties of KB films (b); FT-IR spectra of KB films (c); and the effect of BC dosage on the water vapor permeability and oxygen permeability of KB films (d).

increase their intermolecular force, thus reducing the vibrational frequency of O–H and eventually reducing the wavenumber of the hydroxyl group peak.[44] A similar phenomenon was also reported from the preparation of TP and calcium alginate composite films.[45] Furthermore, the elongation at break (EAB) of the KB films improved from $28.83 \pm 0.17\%$ to $38.17 \pm 0.43\%$ upon increasing the weight ratio of BC to KGM from 0% to 5%, whereas it slightly decreased to $30.19 \pm 0.55\%$ when the weight ratio of BC was further increased to 25%. This result was probably because the addition of BC into the KGM matrix would inhibit the movement of KGM polymeric chains in the film and generate more rigid structures in the film.[25]

The water vapor and oxygen barrier properties are essential in packaging films to preserve the freshness of foodstuffs. The effect of BC dosage on the WVP and OP of KB films was evaluated, and the results are shown in Fig. 2d. When the dosage of BC was increased from 0% to 15%, the WVP and OP values decreased from $(3.87 \pm 0.13) \times 10^{-13}$ to $(3.65 \pm 0.02) \times 10^{-13}$ $g\ cm^{-1}\ s^{-1}\ Pa^{-1}$ and from $(1.45 \pm 0.08) \times 10^{-3}$ to $(0.86 \pm 0.03) \times 10^{-3}\ g\ m^{-1}\ s^{-1}\ Pa^{-1}$, respectively. This behaviour may be attributed to the formation of hydrogen bonds between the hydroxyl groups of BC and the hydroxyl or acetyl groups of KGM in the KB film, which could reduce the amount of free hydroxyl groups in the film, enhancing the physical entanglement between molecular chains and thereby generating dense and continuous networks in the film.[33] However, upon increasing the weight ratio of BC to KGM from 15% to 25%, the WVP and OP values of the KB film were increased from $(3.65 \pm 0.02) \times 10^{-13}$ to $(3.78 \pm 0.03) \times 10^{-13}\ g\ cm^{-1}\ s^{-1}\ Pa^{-1}$ and from $(0.86 \pm 0.03) \times 10^{-3}$ to $(0.99 \pm 0.06) \times 10^{-3}\ g\ m^{-1}\ s^{-1}\ Pa^{-1}$, respectively, which did not help the preservation abilities of KB films. The increase in the WVP value was mainly because an excessive amount of BC could enlarge the concentration of free hydroxyl groups in the film and provide active sites for adsorbing water molecules.[46] Meanwhile, excess BC possibly aggregated in the

film and thus enhanced the porosity of the film, which could offer pathways for oxygen permeation and eventually enhance the OP value of KB film.[47] Therefore, KB film prepared with a 15% weight ratio of BC to KGM was selected for further analysis.

3.2. Structural, mechanical, barrier and antioxidant properties of the KBT films

The influence of the TP weight ratio on the mechanical characteristics of KGM-BC-TP (KBT) films is evaluated, and the results are shown in Fig. 3a and b. The presence of TP resulted in significant differences in the TS and EAB values of the KBT films ($p < 0.05$). Upon increasing the weight ratio of TP to KGM from 0% to 5%, the TS and EAB values of KBT film were gradually elevated from 61.01 ± 1.10 MPa and $28.95 \pm 0.17\%$ to 66.53 ± 0.38 MPa and $39.87 \pm 0.58\%$, respectively. The elevation created a combination of high strength and moderate flexibility that met the requirements for industrial handling and sealing. This elevation was due to hydrogen bond formation between TP and the KB matrix, which was also confirmed by the shifting of the O–H stretching vibration peak from 3415 cm^{-1} to 3400 cm^{-1}, as shown in Fig. 3c. However, upon further enlarging the weight ratio of TP to KGM to 9%, the TS and EAB values of KBT film were reduced to 59.52 ± 0.27 MPa and $33.57 \pm 0.91\%$. This phenomenon was probably due to the fact that the excessive incorporation of TP into the KB matrix would generate more free particles of TP in the film and thus weaken the interactions in the network structure.[30] A similar phenomenon was also noted during the preparation of sodium alginate/ konjac glucomannan/tea polyphenol composite films.[48] The mechanical properties of the KBT films were compared with previously reported polysaccharide-based films, and the results are shown in Table S1. KBT_5 film exhibited a tensile strength of 66.53 ± 0.38 MPa and an elongation at break of $39.87 \pm 0.58\%$. Although its tensile strength showed a certain gap compared to those of KNT and K_8E_2 films, its overall performance surpassed most reported polysaccharide-based films, demonstrating great potential for food packaging applications. Meanwhile, the stable shear viscosity values of film-forming solutions
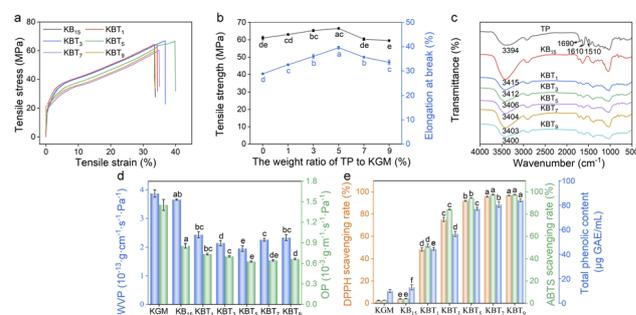

Fig. 3 Tensile stress−strain curves of KBT films (a); the effect of TP dosage on the mechanical properties of KBT films (b); FT-IR spectra of KBT films (c); water vapor permeability and oxygen permeability of KBT films (d); and DPPH and ABTS radical scavenging activities and total phenolic content of KBT films (e).

© 2026 The Author(s). Published by the Royal Society of Chemistry

containing various TP concentrations (1–9% w/w) were examined as a function of the shear rate. As shown in Fig. S1, the viscosity of all solutions obviously decreased upon enlarging the shear rate, indicating the shear thinning behavior typical of non-Newtonian fluids. Furthermore, increasing the vibration frequency (Hz) also enlarged the G' and G'' values. These results were attributed to the idea that increasing the shear rate could disrupt the entanglements between macromolecular chains, which was consistent with previous results.[33]

The effect of TP dosage on the WVP and OP values of the KB films is presented in Fig. 3d. The WVP value of KBT film decreased from $(2.43 \pm 0.11) \times 10^{-13}$ to $(1.95 \pm 0.10) \times 10^{-13}$ g cm^{-1} s^{-1} Pa^{-1} upon increasing the TP content from 1% to 5%, which was due to the formation of hydrogen bonds between TP and the KB film, resulting in a denser structure and preventing the penetration of water vapor. However, the WVP value of KBT film increased to $(2.32 \pm 0.11) \times 10^{-13}$ g cm^{-1} s^{-1} Pa^{-1} when the TP content in the KB film was further increased to 9%. This was attributed to the idea that excessive TP would provide numerous phenolic hydroxyl groups, which would result in increased film hydrophilicity, thus reducing the WVP properties of the film.[49] The OP values of KBT films exhibited a similar trend to that of the WVP values, with a lowest value of $(0.63 \pm 0.10) \times 10^{-3}$ g m^{-1} s^{-1} Pa^{-1}, confirming that KBT film with 5% TP content displayed excellent oxygen barrier properties.

The ABTS and DPPH radical-scavenging rates of the KGM, KB$_{15}$ and KBT films are depicted in Fig. 3e. The DPPH radical scavenging rates of KGM and KB$_{15}$ films were $2.60 \pm 0.24\%$ and $2.70 \pm 0.03\%$, respectively, while their ABTS radical scavenging rates were $3.86 \pm 0.30\%$ and $4.11 \pm 0.23\%$, which confirmed the weak antioxidant capacities of these films. With an increase in TP content, the DPPH and ABTS radical scavenging rates of the composite films increased significantly ($P < 0.05$). When the amount of TP was changed from 1% to 5%, the DPPH radical scavenging rate of KBT film was enhanced from $48.44 \pm 1.48\%$ to $96.74 \pm 0.22\%$ and the ABTS radical scavenging rate was increased from $51.92 \pm 1.41\%$ to $97.50 \pm 0.36\%$. This phenomenon was due to the fact that TP are rich in phenolic hydroxyl groups, which provided excellent scavenging abilities toward free radicals and the trapping of reactive oxygen species, resulting in the excellent antioxidant properties of KBT films. Further elevating the weight ratio of TP to KGM from 5% to 9% caused minor changes in the DPPH and ABTS radical scavenging rates. Subsequently, the TPC in KBT films was measured. As shown in Fig. 3e and S2, the TPC sharply increased from KBT$_1$ to KBT$_5$ and then exhibited minor changes from KBT$_5$ to KBT$_9$. The trend of TPC changes was consistent with the DPPH and ABTS radical scavenging capacities. KBT$_5$ exhibited the highest TPC of 80.85 µg GAE per mL and thus was selected for further analysis. Therefore, KBT film with a 5% weight ratio of TP was selected for further analysis.

3.3. Morphological and physicochemical characterization of KGM, KB$_{15}$ and KBT$_5$ films

The surface and cross-sectional morphologies of KGM, KB$_{15}$ and KBT$_5$ films were observed using SEM, and the images are depicted in Fig. 4a. As shown in Fig. 4a(I) and (IV), pure KGM film exhibited a smooth, uniform and flat surface, and a cross-section without holes or cracks. However, the KB$_{15}$ film surface was wrinkled and its cross-section surface exhibited a distinctive groove morphology, as illustrated in Fig. 4a(II) and (V). Numerous hydrogen bonds could be formed through the connection of hydroxyl groups in BC with hydroxyl groups or acetyl groups in KGM, which could restrict the movement of the molecular chains in the film, resulting in the formation of wrinkled structures.[50] As shown in Fig. 4a(III) and (VI), a morphology with wrinkles and gullies on the surface was seen and the cross-section of the KBT films could be weakened after the incorporation of TP into the films, which was probably due to the formation of hydrogen bonds between the phenolic hydroxyl groups of TP and the hydroxyl groups of KB$_{15}$; this could inhibit shrinkage of the film and result in a structurally uniform film[51]. Furthermore, the surface and cross-section images of KBT films did not exhibit large particles or phase separation. This result indicated that the diverse materials (KGM, BC, and TP) were uniformly dispersed in the film matrix.

The thermal stability of KGM, KB$_{15}$ and KBT$_5$ films was also evaluated through thermogravimetric analysis (TGA), and the curves are shown in Fig. 4b. Mass loss from these three films occurred in three stages. The first stage took place from room temperature to 125 °C, which was mainly due to the evaporation of bound water from the films.[52] The second stage occurred from
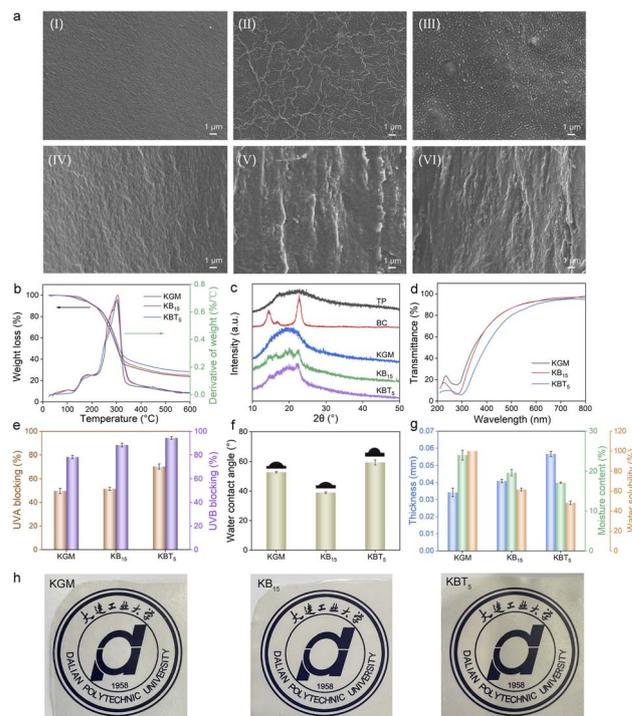

Fig. 4 Morphological and physicochemical characterization of KGM, KB$_{15}$ and KBT$_5$ films: surface and cross-sectional SEM images of KGM (I and IV), KB$_{15}$ (II and V) and KBT$_5$ (III and VI) (a); TGA and DTGA curves (b); XRD patterns (c); UV-vis light transmittance spectra (d); UVA and UVB blocking rates (e); water contact angles (f); thickness and water sensitivity values (g); and photographs (h).

125 °C to 220 °C and was mainly associated with the thermal degradation of glycerol in the film.[33] The third stage generally ranged from 220 °C to 340 °C; this was the main weight loss stage of films and was primarily due to the degradation and depolymerization of the sugar rings in KGM.[53] The temperatures at 50% weight loss for KGM, KB_{15}, and KBT_5 films were 300.23 °C, 305.39 °C, and 310.25 °C, while their temperatures at maximum weight loss were 298.88 °C, 303.15 °C, and 303.51 °C, respectively. It can be concluded that the incorporation of BC and TP could enhance the thermal stability of KGM films due to the formation of hydrogen bonds between them. The XRD patterns of KGM, KB_{15} and KBT_5 films are presented in Fig. 4c. Pure KGM film and TP both exhibited typical amorphous states.[33] The XRD pattern of BC displayed three distinct crystalline peaks at 2θ values of 14.36°, 16.74° and 22.75°, corresponding to the (101), (10$\bar{1}$) and (002) crystal planes, respectively.[33] These three peaks were also observed in the XRD pattern of KB_{15} film, indicating that BC had been successfully incorporated into the structure of KGM. When TP were incorporated into the KB_{15} matrix, the diffraction peaks in the XRD spectrum of the KBT_5 film flattened further, indicating a reduction in the apparent crystallinity of the BC-containing domains.

Fig. 4d displays the UV-visible transmittance spectra of KGM, KB_{15} and KBT_5 films in the range of 200 to 800 nm. The transmittance values of KGM, KB_{15} and KBT_5 films at 600 nm were 93.19%, 93.09% and 90.29%, respectively, and the opacity values were 0.61 ± 0.06, 0.74 ± 0.03, 1.08 ± 0.02, respectively (Table 1). These results confirmed that the transparency of KGM films could be reduced after the incorporation of BC and TP. However, the KBT_5 film exhibited transmittance exceeding 90% at a wavelength of 600 nm. This high transparency is particularly crucial in the retail sector, as it allows consumers to assess product freshness without the need to open the packaging. The UV shielding properties of the films were assessed based on their UVA and UVB ultraviolet shielding performance. As presented in Fig. 4e, the UVA and UVB shielding rates of pure KGM film were 41.07% and 77.31%, respectively, which were increased to 78.28% to 88.36% for the KB_{15} film, suggesting that the UV shielding performance of KGM film was significantly improved by the multiple scattering effects of BC nanofiller, as it has a three-dimensional porous network structure.[54] Additionally, the incorporation of TP also had a positive effect on the UV blocking properties of KBT_5 film, whose UVA and UVB shielding rates were 70.44% and 94.36%, respectively. These results indicated that KBT_5 film has excellent UV shielding ability and could be effective in preventing UV-induced lipid oxidation for specific food-packaging applications.

The wettability and hydrophilicity of film surfaces are generally characterized using the water contact angles. As illustrated in Fig. 4f, the WCA of pure KGM film was $52.80 \pm 0.46°$, while the WCA of KB_{15} film was further reduced to $39.00 \pm 0.55°$, which was attributed to the abundant hydrophilic hydroxyl groups of BC. Compared with KB_{15} film, the WCA of KBT_5 was enhanced to $59.46 \pm 1.71°$ due to the hydrophobic benzene ring groups in TP.[55] Therefore, BC incorporation increased the surface hydrophilicity of the film, whereas subsequent TP addition decreased its hydrophilicity, indicating opposite contributions of BC and TP to wettability. Typically, hydrophilic components in a film matrix readily form hydrogen bonds with water molecules, facilitating the adsorption and diffusion of water vapor and thus increasing WVP. In contrast, hydrophobic segments can block the continuous transmission of polar molecules, thereby reducing WVP and OTR.[56] With the introduction of TP, KBT_5 exhibited superior hydrophobicity compared to KB_{15}. Moreover, the OP and WVP values of KBT_5 are lower than those of KB_{15}, indicating that the improvement in hydrophobicity was beneficial for enhancing the barrier properties of the film. Furthermore, the MC and WS values of KGM film were $24.02 \pm 0.01\%$ and 100%, respectively, confirming that the KGM film had poor water resistance. The moisture content values of KB_{15} and KBT_5 films were reduced to $19.65 \pm 0.01\%$ and $17.11 \pm 0.01\%$, while the water solubility values were decreased to $61.72 \pm 1.47\%$ and $48.26 \pm 1.81\%$, respectively. These results confirmed that the films containing BC and TP displayed higher water resistance than pure KGM film.

The color results for the KGM, KB_{15} and KBT_5 films are listed in Table 1. After the introduction of BC into the KGM matrix, the L^* value of KB_{15} film was decreased from 92.24 to 90.93, while the a^* and b^* values scarcely changed. The findings demonstrated that the incorporation of BC did not markedly alter the color properties of the KGM film. Nevertheless, compared with KB_{15}, the L^* value of KBT_5 film was significantly reduced to 88.42 ± 0.11, while the a^* and b^* values were enhanced to -0.03 ± 0.03 and 5.63 ± 0.02, respectively. This phenomenon was attributed to the inherent yellowish-brown color of TP. The transmittance of KBT_5 film was excellent, and patterns and letters underneath were clearly visible (Fig. 4h).

3.4. Release behavior

The release behavior of TP from KBT_5 film in different food simulants was divided into two stages: the initial burst release stage within 30 minutes and the slowed release stage after 30 minutes. The equilibrium release efficiencies in 50% ethanol and deionized water were 78.80% and 66.74%, respectively

Table 1 The optical properties of KGM, KB_{15} and KBT_5 films

Sample	Opacity	L^*	a^*	b^*	ΔE^*
KGM	0.61 ± 0.06^c	92.24 ± 0.09^a	-0.98 ± 0.01^b	-0.35 ± 0.08^b	6.25 ± 0.12^c
KB15	0.74 ± 0.03^b	90.93 ± 0.12^b	-0.97 ± 0.01^b	-0.39 ± 0.03^c	7.52 ± 0.11^b
KBT5	1.08 ± 0.02^a	88.42 ± 0.11^c	-0.03 ± 0.03^a	5.63 ± 0.02^a	11.45 ± 0.10^a

[a] Note: values are presented as mean $\pm$ SD ($n = 3$). Different superscript letters (a–c) within the same column indicate significant differences ($p < 0.05$).

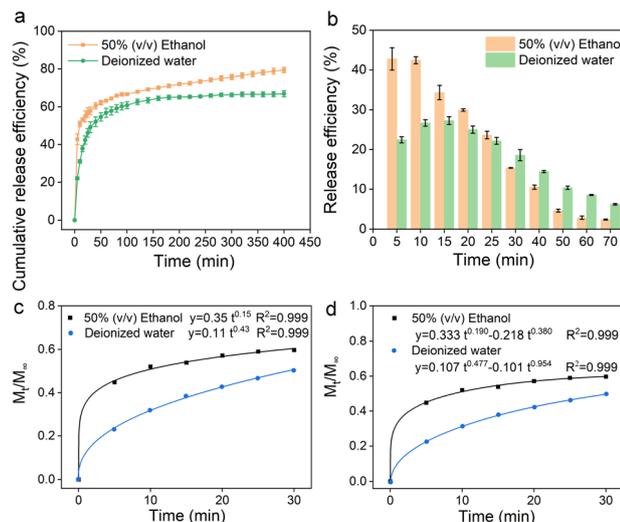**Fig. 5** The release of TP from KBT$_5$ film in 50% ethanol and deionized water: cumulative release curves (a); release efficiency at each testing point over 70 minutes (b); and fitting of the experimental data by Ritger–Peppas (c) and Peppas–Sahlin models (d).

(Fig. 5a), while the corresponding release rates after 5 minutes were 42.78% and 22.46% (Fig. 5b). It can be concluded that the release behavior of TP in the 50% ethanol simulation solution was faster than that in deionized water, corresponding to the better affinity of TP with ethanol simulation solution than with water. Consequently, the higher release in 50% ethanol indicated more rapid antioxidant delivery to lipophilic food matrices. To investigate the release mechanism, the experimental release data were analyzed using the Ritger–Peppas and Peppas–Sahlin models. As shown in Fig. 5c and d, the release indices (n) from the Ritger–Peppas model were below 0.45, whereas the $|k_1/k_2|$ values from the Peppas–Sahlin model were more than 1.0. These results indicated that the release of TP from the film was well described by the Fickian diffusion mechanism,[38] which is related to the difference in the concentration of TP inside and outside the film.

3.5. Application of KBT films to fruit preservation

Freshly cut apples were selected to evaluate the antioxidant properties of the films because they are a common fruit susceptible to oxidative browning. In this study, fresh-cut apple slices were selected to investigate the freshness preservation performance of KBT films, and they were packaged separately using KB$_{15}$, KBT$_5$ and commercially available films. Unpackaged fruit served as a control group. The preservation of freshness by the films was assessed by evaluating the weight loss, pH, color parameters, TTA and PPO activities of fresh-cut apples. The results are shown in Fig. 6. As shown in Fig. 6b, the weight loss of fresh-cut apples varied significantly depending on the packaging. After one week, the weight loss of unpackaged apples (41.04 ± 1.15%) was significantly higher than those of the packaged groups. During the same period, the weight loss rate of KBT$_5$ (20.72 ± 0.80%) was markedly lower than that of KB$_{15}$ (30.87 ± 0.63%). Therefore, the KBT$_5$ film exhibited the best performance in preventing water vapor transmission
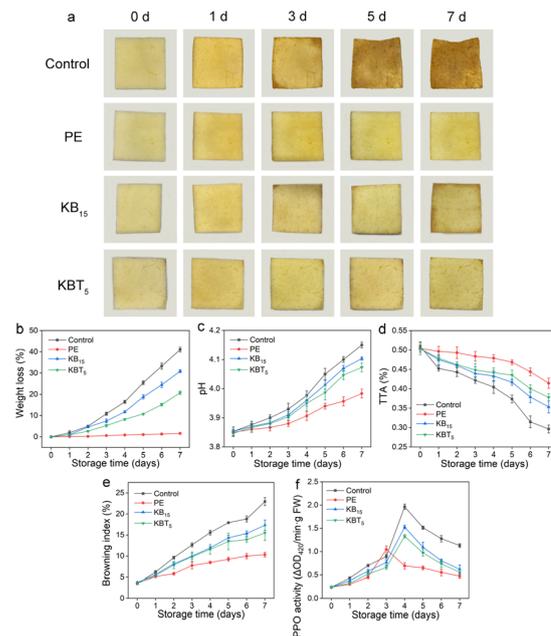

Fig. 6 The effect of PE, KB$_{15}$ and KBT$_5$ films on the physicochemical properties of fresh-cut apples: the appearance of fresh-cut apples (a), weight loss data (b), pH values (c), total titratable acid (TTA) data (d), browning indices (e), and PPO activities (f).

among these biodegradable films, as evidenced by its noticeably lower weight loss compared to the KB$_{15}$ film. Over 7 days of storage, all experimental groups of fresh-cut apples showed a gradually increasing pH value (Fig. 6c); the pH value of fresh-cut apples treated with KBT$_5$ (4.07 ± 0.02) was close to that of the PE group (3.98 ± 0.02), and lower than both the control group and KB$_{15}$. Throughout the storage period, the TTA values (Fig. 6d) exhibited a decreasing trend. After 7 days of storage, the TTA values decreased from an initial value of 0.50 ± 0.01% to 0.30 ± 0.01% in the control group, 0.42 ± 0.01% in the PE group, 0.35 ± 0.02% in the KB$_{15}$ group, and 0.38 ± 0.01% in the KBT$_5$ group, owing to the depletion of organic acids (*e.g.*, malic acid, citric acid, *etc.*) which served as respiratory substrates in the respiration of apples during storage[57]. In addition, as shown in Fig. 6e and f, compared with the control (22.94 ± 0.95%; 1.13 ± 0.04) and KB$_{15}$ film (17.33 ± 1.20%; 0.62 ± 0.09) groups, the fresh-cut apples wrapped with KBT$_5$ film exhibited smaller changes in BI and PPO activities (15.47 ± 1.75%; 0.57 ± 0.05), with values closer to those observed in the PE group, indicating that the antioxidant performance of KBT$_5$ film effectively inhibited the browning of fresh-cut apples. Meanwhile, the digital images in Fig. 6a further confirmed that apples enclosed with KBT$_5$ film retained better freshness than those packaged with KB$_{15}$ film or left untreated. Therefore, KBT$_5$ film effectively retarded the respiration rate of apples and was beneficial for maintaining the quality of fresh-cut apples.

3.6. Biodegradability, cytotoxicity and seed germination experiments involving KB$_{15}$ and KBT$_5$ films

Fig. 7a illustrates the macroscopic appearance changes of the composite films over time in the natural environment. The KB$_{15}$

and KBT$_5$ films were mostly degraded on the 28th day, which was mainly due to the action of microorganisms (bacteria, fungi and actinomycetes) in the soil.[41] Contrastingly, the PE film retained its structure throughout the degradation testing process and was without any visible degradation. To quantitatively assess biodegradability, the mass loss of the films was measured at regular intervals (Fig. S3). The results showed that the KB$_{15}$ and KBT$_5$ films underwent rapid degradation, with mass loss exceeding 90% by day 28. In contrast, the mass of the PE film exhibited negligible changes during the overall degradation testing process. It was clear that these mass loss changes were consistent with the visual observations presented in Fig. 7a. Therefore, the composite films exhibited excellent biodegradability in natural environments. The biosafety of the composite films was evaluated by examining their effect on the viability of 3T3 and HUVEC cells using the MTT assay, and the corresponding results are shown in Fig. 7b. Almost 100% of 3T3 and HUVEC cells survived after co-incubation with KB$_{15}$ and KBT$_5$ films for 24 hours. Furthermore, as shown in Fig. 7c and d, no dead cells were observed, and all cells were alive.

The impact of degraded film on plant growth was assessed by comparing the growth of seasonal cabbages grown in soil with degraded PE, KB$_{15}$ and KBT$_5$ films, as illustrated in Fig. 8a and b. After 21 days of incubation, the germination percentages of seasonal cabbage planted in soil with degraded KB$_{15}$ and KBT$_5$ films were 81.45% and 82.22%, respectively (Fig. 8c). The germination rates of the experimental groups were similar to those of the control group (87.38%) and significantly superior to the 31.91% germination rate of the PE group. Meanwhile, the average plant heights of the KB$_{15}$ and KBT$_5$ film groups were not significantly different from those in the control group, suggesting that the composite films had no significant influence on plant growth (Fig. 8d).

The combination of high-efficiency freshness preservation, rapid biodegradability, and non-toxic degradation byproducts demonstrated the immense potential of this composite film for addressing key challenges relating to sustainable industrial food packaging.
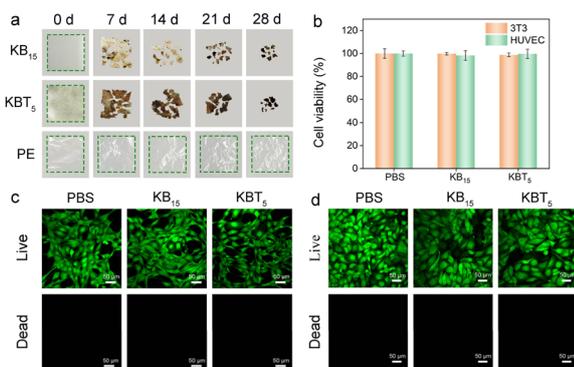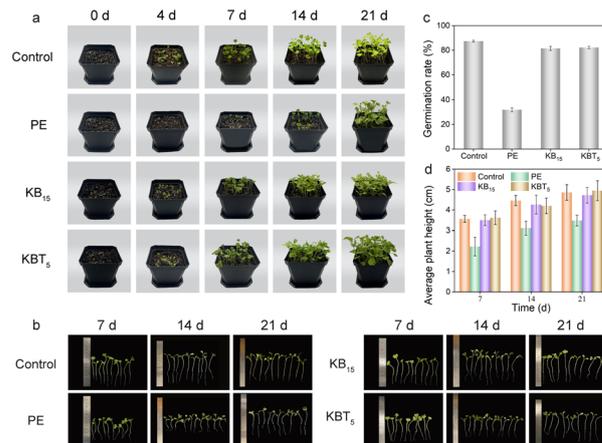

Fig. 8 Images of seasonal cabbage seeds grown in film–degraded soil for 21 days (a); comparison of seasonal cabbage germination in soil degraded by different films (b); germination rate of seasonal cabbage seeds in soil degraded by different films (c); height increase of seasonal cabbage in soil after degradation of different films (d).

4 Conclusions

In this study, a biodegradable food packaging film (KBT) was developed using food-grade raw materials and a water-based solution casting method, making it suitable for large-scale industrial production. The effect of BC dosage on the mechanical and barrier properties of KGM-based films and the influence of TP content on the physical and antioxidant properties of the resulting KGM-BC composite films were investigated. The incorporation of BC into KGM films significantly improved their mechanical properties, which is mainly attributed to the hydrogen bonds formed between the hydroxyl groups of BC and the hydroxyl or acetyl groups of KGM. The addition of TP gave the KGM-BC film excellent mechanical strength, and antioxidant, UV shielding and barrier properties. The application of KGM-BC-TP film as a packaging material for the preservation of fresh-cut apples was effective in reducing weight loss and the browning index, thereby contributing to an extended shelf life. KGM-BC-TP film largely degraded after being buried in natural soil for 28 days, confirming its excellent biodegradability. Furthermore, the film exhibited non-toxicity toward 3T3 and HUVEC cells and non-adverse effects on plant growth, demonstrating its high biocompatibility. In conclusion, the developed KGM-BC-TP film was not only a stable and effective packaging material for food preservation but also a viable alternative to polyethylene. It effectively addressed key industrial challenges related to functionality and sustainability. These efforts will advance KGM-BC-TP from laboratory validation toward industrial packaging systems, positioning it as an ideal choice for next-generation eco-friendly food packaging.

Author contributions

Lan Ma: writing – original draft, data curation, conceptualization. Pengyu Hu: writing – review & editing, methodology. Yihao

Fig. 7 The biodegradability and cytotoxicity of different films. The biodegradability of PE, KB15 and KBT5 films in natural soil (a); the cytotoxicity of KB15 and KBT5 films toward 3T3 and HUVEC cells, respectively (b); and fluorescence images of 3T3 fibroblasts (c) and HUVEC cells (d).

Zhang: writing – review & editing. Yunchuan Dai: writing – review & editing. Yanzhu Guo: writing – review & editing, supervision, project administration, conceptualization.

Conflicts of interest

The authors declare no conflicts of interest.

Data availability

The data supporting this article have been included as part of the supplementary information (SI). Supplementary information: figures and tables which are related to the rheological behavior and biodegradation data of the composited films, the gallic acid standard curve, and the comparison of mechanical properties between our films and reported similarly materials. See DOI: https://doi.org/10.1039/d5ra07243c.

Acknowledgements

References

1 Y. Wang, K. Liu, M. Zhang, T. Xu, H. Du, B. Pang and C. Si, *Carbohydr. Polym.*, 2023, **313**, 120851.

2 A. S. Khandeparkar, R. Paul, A. Sridhar, V. V. Lakshmaiah and P. Nagella, *Sustain. Chem. Pharm.*, 2024, **39**, 101579.

3 M. Zhao, P. Han, H. Mu, S. Sun, J. Dong, J. Sun, S. Lu, Q. Wang and H. Ji, *Food Chem.:X*, 2025, **25**, 102174.

4 U. Tukenmez Emre, S. Sirin, S. Nigdelioglu Dolanbay and B. Aslim, *Polym. Bull.*, 2025, **82**, 2779–2825.

5 L. S. Devi, A. K. Jaiswal and S. Jaiswal, *Curr. Res. Food Sci.*, 2024, **8**, 100720.

6 S. A. A. Mohamed, M. El-Sakhawy and M. A.-M. El-Sakhawy, *Carbohydr. Polym.*, 2020, **238**, 116178.

7 K. Zhuang, X. Shu and W. Xie, *Carbohydr. Polym.*, 2024, **344**, 122503.

8 D. U. Kapoor, H. Sharma, R. Maheshwari, A. Pareek, M. Gaur, B. G. Prajapati, G. R. Castro, K. Thanawuth, S. Suttiruengwong and P. Sriamornsak, *Carbohydr. Polym.*, 2024, **339**, 122266.

9 S. Wang, D. Zhuang, R. Li, Z. Liu and J. Zhu, *Int. J. Biol. Macromol.*, 2024, **264**, 130483.

10 Y. Du, Y. Zhang and J. Pang, *Food Biosci.*, 2024, **61**, 104544.

11 C. Chandarana, S. Bonde, V. Vashi, M. S. Akhter and B. Prajapati, *J. Food Process. Eng.*, 2024, **47**, e70009.

12 L. Zhou, D. Zhang, N. Bu, L. Huang, H. Lin, W. Liu, G. Cao, R. Mu, J. Pang and L. Wang, *Int. J. Biol. Macromol.*, 2024, **266**, 131250.

13 Y. Kawahara, M. Nakagawa and M. Yamamoto, *J. Macromol. Sci., Part B: Phys.*, 2021, **60**, 947–956.

14 X. Wang, Y. Chen, X. Zhao and J. Pang, *Foods*, 2025, **14**, 1563.

15 W. Sun, Y. Yao, J. Ju, H. Yuan and Y. Tan, *ACS Appl. Polym. Mater.*, 2025, **7**, 5003–5012.

16 Y. Jin and Z. Lu, *Polym. Bull.*, 2024, **81**, 1373–1388.

17 Z. Bian, X. Li, J. Zhang, M. Shi, Z. Xin, H. Wang, S. Komarneni, K. Zhang, Z. Ni and G. Hu, *Food Hydrocoll.*, 2024, **151**, 109767.

18 N. Duan, Q. Li, X. Meng, Z. Wang and S. Wu, *Food Chem.*, 2021, **364**, 130441.

19 Z. Lin, S. Bi, G. Du, Y. Zhang, H. Fu, L. Fu, C. Xu and B. Lin, *ACS Sustain. Chem. Eng.*, 2023, **11**, 12747–12758.

20 A. Nesic, S. Meseldzija, G. Cabrera-Barjas and A. Onjia, *Foods*, 2022, **11**, 360.

21 N. Halib, I. Ahmad, M. Grassi and G. Grassi, *Int. J. Pharm.*, 2019, **566**, 631–640.

22 F. A. G. S. Silva, S. Branco, F. Dourado, B. Neto and M. Gama, *J. Clean. Prod.*, 2025, **493**, 144876.

23 Y. Zhang, G. Chen, W. Qin, X. Men, L. Liu, Y. Zhang, Q. Li, L. Wang and H. Zhang, *ACS Appl. Mater. Interfaces*, 2023, **15**, 44354–44363.

24 L. Rosson, B. Tan, W. Best and N. Byrne, *Cellulose*, 2024, **31**, 10165–10190.

25 X. Wang, C. Guo, W. Hao, N. Ullah, L. Chen, Z. Li and X. Feng, *Int. J. Biol. Macromol.*, 2018, **118**, 722–730.

26 Z. Shao, W. Lan and J. Xie, *Food Chem.*, 2025, **478**, 143604.

27 C. Chen, S. Deng, H. Tian, H. Yu, J. Huang, X. Lou and H. Yuan, *Food Hydrocoll.*, 2025, **165**, 111267.

28 N. Li, X. Yang and D. Lin, *Food Packag. Shelf Life*, 2022, **34**, 100989.

29 V. M. Rangaraj, K. Rambabu, F. Banat and V. Mittal, *Food Biosci.*, 2021, **43**, 101251.

30 M. Ma, M. Gu, S. Zhang and Y. Yuan, *Int. J. Biol. Macromol.*, 2024, **259**, 129267.

31 K. Takács, M. Á. Németh, T. Renkecz, D. Tátraaljai and B. Pukánszky, *Polym. Degrad. Stab.*, 2024, **230**, 111046.

32 S. C. Forester and J. D. Lambert, *Mol. Nutr. Food Res.*, 2011, **55**, 844–854.

33 Z. Liu, D. Lin, P. Lopez-Sanchez and X. Yang, *Int. J. Biol. Macromol.*, 2020, **145**, 634–645.

34 M. J. Mehta and A. Kumar, *ACS Sustain. Chem. Eng.*, 2019, **7**, 8631–8636.

35 Y. Cao, Z. Song, W. Ni, Y. Ma, K. Xin, Q. Yu and L. Zhang, *Food Hydrocoll.*, 2024, **155**, 110224.

36 F. Yi, X. Chen, F. Hou, L. Song, S. Zhan, X. Wang, R. Zhang, Q. Yang, X. Wang and Z. Liu, *Int. J. Biol. Macromol.*, 2024, **269**, 131970.

37 Z. Alinaqi, A. Khezri and H. Rezaeinia, *Int. J. Biol. Macromol.*, 2021, **173**, 193–202.

38 Z. Miao, R. Lv, S. Teng, C. Cao and P. Lu, *Int. J. Biol. Macromol.*, 2022, **222**, 403–412.

39 X. Ma, J. Feng, Y. Zhou, L. Wang, Y. He and H. Zhang, *Int. J. Food Sci. Technol.*, 2024, **59**, 9051–9059.

40 T. Du, X. Li, S. Wang, Z. Su, H. sun, J. Wang and W. Zhang, *Food Res. Int.*, 2023, **163**, 112293.

41 Q. Wang, Y. Duan, Y. Huang, Y. Teng, C. Li, Y. Tao, J. Lu, J. Du and H. Wang, *Carbohydr. Polym.*, 2024, **323**, 121410.

42 M. D. Silva, J. V. Ernesto, A. R. Rinaldi, A. P. Noletto, P. S. Lopes, R. A. Carvalho, V. A. Garcia and C. M. Yoshida, *Polymers*, 2025, **17**, 473.

43 A. G. De Souza, R. R. Ferreira, J. Harada and D. S. Rosa, *J. Appl. Polym. Sci.*, 2021, **138**, 50020.

44 L. Dou, B. Li, K. Zhang, X. Chu and H. Hou, *Int. J. Biol. Macromol.*, 2018, **118**, 1377–1383.

45 Y. Biao, C. Yuxuan, T. Qi, Y. Ziqi, Z. Yourong, D. J. McClements and C. Chongjiang, *Food Hydrocoll.*, 2019, **97**, 105197.

46 S. Yadav, G. Mehrotra, P. Bhartiya, A. Singh and P. Dutta, *Carbohydr. Polym.*, 2020, **227**, 115348.

47 X. Wang, Y. Xie, H. Ge, L. Chen, J. Wang, S. Zhang, Y. Guo, Z. Li and X. Feng, *Carbohydr. Polym.*, 2018, **179**, 207–220.

48 S. Wang, M. Li, B. He, Y. Yong and J. Zhu, *Int. J. Biol. Macromol.*, 2023, **242**, 124732.

49 Y. Lei, H. Wu, C. Jiao, Y. Jiang, R. Liu, D. Xiao, J. Lu, Z. Zhang, G. Shen and S. Li, *Food Hydrocoll.*, 2019, **94**, 128–135.

50 H. Yang, Z. Xu, L. Li, C. Li, Y. Tao, J. Lu, J. Hu, X. Xia, M. Tan, J. Du and H. Wang, *Food Hydrocoll.*, 2025, **158**, 110490.

51 R. Luo, Z. Peng, N. Wu, L. Zhang, B. Peng, R. Shao, W. Xu and L. Yang, *Int. J. Biol. Macromol.*, 2024, **281**, 135867.

52 T. Nisar, Z.-C. Wang, X. Yang, Y. Tian, M. Iqbal and Y. Guo, *Int. J. Biol. Macromol.*, 2018, **106**, 670–680.

53 W. Lin, Y. Ni and J. Pang, *Carbohydr. Polym.*, 2019, **222**, 114986.

54 Y.-C. Ding, G.-W. Tang, H.-Y. Zhao, J.-M. Liu, T.-H. Fan, Y.-C. Peng, P. J. Ker and D.-S. Geng, *ACS Appl. Mater. Interfaces*, 2025, **17**, 6857–6866.

55 W.-M. Song, L.-Y. Zhang, R.-Y. Fan, Y. Liu and Y.-Z. Wang, *Compos. B Eng.*, 2024, **287**, 111848.

56 K. Wu, Q. Zhu, H. Qian, M. Xiao, H. Corke, K. Nishinari and F. Jiang, *Food Hydrocoll.*, 2018, **79**, 301–309.

57 M. Cofelice, F. Lopez and F. Cuomo, *Foods*, 2019, **8**, 189.